

## **Synergistically optimizing electrocatalytic performance of IrO<sub>2</sub> with double doping and bi-directional strains for acidic oxygen evolution reaction**

Xiao Wu<sup>†, §</sup>, Weiwei Han<sup>†, §</sup>, Shaoyun Hao<sup>†</sup>, Yi He<sup>†</sup>, Lecheng Lei<sup>†, ‡</sup>, Xingwang Zhang<sup>\*, †, ‡</sup>

*†Key Laboratory of Biomass Chemical Engineering of Ministry of Education, College of Chemical and*

*Biological Engineering Zhejiang University, Hangzhou 310027, China*

*‡Institute of Zhejiang University-Quzhou, Quzhou 324000, China*

§Xiao Wu and Weiwei Han contribute equally to this work.

\*Corresponding author E-mail: xwzhang@zju.edu.cn

## Contents

<b>Experimental section</b> .....	S4
<b>Supplementary Figure 1.</b> TEM image, the HR-TEM image of IrO <sub>x</sub> and the corresponding elemental mapping of IrO <sub>x</sub> .....	S9
<b>Supplementary Figure 2.</b> TEM image, the HR-TEM image of Sb <sub>0.2</sub> Ir <sub>0.8</sub> O <sub>x</sub> @TB-IrO <sub>x</sub> , TEM-EDS line scan analysis and the corresponding elemental mapping of Sb <sub>0.2</sub> Ir <sub>0.8</sub> O <sub>x</sub> @TB-IrO <sub>x</sub> .....	S10
<b>Supplementary Figure 3.</b> TEM image, the HR-TEM image of Tm <sub>0.1</sub> Ir <sub>0.9</sub> O <sub>x</sub> @TB-IrO <sub>x</sub> and the corresponding elemental mapping of Tm <sub>0.1</sub> Ir <sub>0.9</sub> O <sub>x</sub> @TB-IrO <sub>x</sub> .....	S11
<b>Supplementary Figure 4.</b> XRD patterns of TB-IrO <sub>x</sub> , Tm <sub>0.1</sub> Ir <sub>0.9</sub> O <sub>x</sub> @TB-IrO <sub>x</sub> , Sb <sub>0.2</sub> Ir <sub>0.8</sub> O <sub>x</sub> @TB-IrO <sub>x</sub> and Tm <sub>0.1</sub> Sb <sub>0.2</sub> Ir <sub>0.7</sub> O <sub>x</sub> @TB-IrO <sub>x</sub> nanocatalysts.....	S12
<b>Supplementary Table 1.</b> The percentages of various valence state Ir in the various nanocatalysts.....	S13
<b>Supplementary Figure 5.</b> Electrochemical performance of various synthesized Tm <sub>n</sub> Sb <sub>m</sub> Ir <sub>1-m-n</sub> O <sub>x</sub> @TB-IrO <sub>x</sub> nanocatalysts.....	S14
<b>Supplementary Table 2.</b> Comparisons of Tm <sub>0.1</sub> Sb <sub>0.2</sub> Ir <sub>0.7</sub> O <sub>x</sub> @TB-IrO <sub>x</sub> with other representative OER catalysts reported under acidic condition.....	S15
<b>Supplementary Table 3.</b> Comparisons of Tm <sub>0.1</sub> Sb <sub>0.2</sub> Ir <sub>0.7</sub> O <sub>x</sub> @TB-IrO <sub>x</sub> with other representative OER catalysts reported under acidic condition at 100 mA cm <sup>-2</sup> .....	S17
<b>Supplementary Figure 6.</b> CV curves of various nanocatalysts collected at different scan rates in 0.5 M H <sub>2</sub> SO <sub>4</sub> electrolyte.....	S18
<b>Supplementary Table 4.</b> ICP analysis of leached metal elements from the Tm <sub>0.1</sub> Sb <sub>0.2</sub> Ir <sub>0.7</sub> O <sub>x</sub> @TB-IrO <sub>x</sub> after OER stability test in 0.5 M H <sub>2</sub> SO <sub>4</sub> at 10 mA cm <sup>-2</sup> .....	S19
<b>Supplementary Figure 7.</b> TEM image, the HR-TEM image of Tm <sub>0.1</sub> Sb <sub>0.2</sub> Ir <sub>0.7</sub> O <sub>x</sub> @TB-IrO <sub>x</sub> -post reaction and the corresponding elemental mapping of Tm <sub>0.1</sub> Sb <sub>0.2</sub> Ir <sub>0.7</sub> O <sub>x</sub> @TB-IrO <sub>x</sub> -post reaction.....	S20
<b>Supplementary Figure 8.</b> XRD patterns of Tm <sub>0.1</sub> Sb <sub>0.2</sub> Ir <sub>0.7</sub> O <sub>x</sub> @TB-IrO <sub>x</sub> and Tm <sub>0.1</sub> Sb <sub>0.2</sub> Ir <sub>0.7</sub> O <sub>x</sub> @TB-IrO <sub>x</sub> -post reaction nanocatalysts.....	S21
<b>Supplementary Figure 9.</b> Ir 4f XPS spectra for Tm <sub>0.1</sub> Sb <sub>0.2</sub> Ir <sub>0.7</sub> O <sub>x</sub> @TB-IrO <sub>x</sub> and	

$Tm_{0.1}Sb_{0.2}Ir_{0.7}O_x@TB-IrO_x$ -post reaction nanocatalysts.....	S22
<b>Supplementary Figure 10.</b> The free energies calculated at $U = 0$ toward acidic OER reaction steps on the $IrO_x$ and $Tm_{0.1}Ir_{0.9}O_x@IrO_x$ , respectively .....	S23
<b>Supplementary Figure 11.</b> The free energies calculated at $U = 0$ toward acidic OER reaction steps on the $Sb_{0.2}Ir_{0.8}O_x@IrO_x$ and $Tm_{0.1}Sb_{0.2}Ir_{0.7}O_x@IrO_x$ , respectively .....	S24
<b>Supplementary Figure 12.</b> The free energies calculated at $U = 0$ toward acidic OER reaction steps on the TB- $IrO_x$ (1%, 2%, 4%, 6%, 8%), respectively.....	S25
<b>Supplementary Figure 13.</b> The free energies calculated at $U = 0$ toward acidic OER reaction steps on the $Tm_{0.1}Ir_{0.9}O_x@TB-IrO_x$ (1%, 2%, 4%, 6%, 8%), respectively .....	S26
<b>Supplementary Figure 14.</b> The free energies calculated at $U = 0$ toward acidic OER reaction steps on the $Sb_{0.2}Ir_{0.8}O_x@TB-IrO_x$ (1%, 2%, 4%, 6%, 8%), respectively .....	S27
<b>Supplementary Figure 15.</b> The free energies calculated at $U = 0$ toward acidic OER reaction steps on the $Tm_{0.1}Sb_{0.2}Ir_{0.7}O_x@TB-IrO_x$ (1%, 2%, 4%, 6%, 8%), respectively .....	S28
<b>Supplementary Figure 16.</b> Projected density of state (DOS) of $Tm_{0.1}Ir_{0.9}O_x@TB-IrO_x$ (0%, 1%, 2%, 4%, 6%, 8%).....	S29
<b>Supplementary Figure 17.</b> Projected density of state (DOS) of $Sb_{0.2}Ir_{0.8}O_x@TB-IrO_x$ (0%, 1%, 2%, 4%, 6%, 8%).....	S30
<b>Supplementary Figure 18.</b> Projected density of state (DOS) of $Tm_{0.1}Sb_{0.2}Ir_{0.7}O_x@TB-IrO_x$ (0%, 1%, 2%, 4%, 6%, 8%).....	S31
<b>Supplementary Figure 19.</b> Physical picture of PEM electrolytic cell and membrane electrode after operation and disassembly. ....	S32
<b>Supplementary Table 5.</b> Under the condition that all metal atoms are active for OER, the TOF values of various $Tm_nSb_mIr_{1-m}O_x@TB-IrO_x$ anode catalysts in the PEM.....	S33
<b>Supplementary Table 6.</b> Under the condition that only the metal atoms on the particle surface are active for OER, the TOF values of various $Tm_nSb_mIr_{1-m}O_x@TB-IrO_x$ anode catalysts in PEM.....	S34
<b>Supplementary Table 7.</b> The power and efficiency of the PEM electrolyzer employing various $Tm_nSb_mIr_{1-m}O_x@TB-IrO_x$ anode catalysts operated at $2 A cm^{-2}$ .....	S35

## **Experimental section**

### *Preparation of thulium and antimony doped iridium oxide*

The bi-directional  $\text{Tm}_{0.1}\text{Sb}_{0.2}\text{Ir}_{0.7}\text{O}_x@\text{TB-IrO}_x$  catalysts were prepared through a method involving the use of a complexing agent. Iridium (III) acetate (Macklin), Antimony trichloride (Aladdin), and citric acid (Macklin) were employed without any further purification. Initially, Iridium acetate (30 mg) and citric acid (3 mg) were dissolved in 20 mL of ethanol, followed by 30 minutes of ultrasonic treatment. Subsequently, Antimony trichloride (3.76 mg) and Thulium chloride hexahydrate (3.16 mg) was added to the ethanol solution of Iridium acetate, and the mixture was thoroughly sonicated to achieve homogeneity. To adjust the pH to 10, a 0.25 mol L<sup>-1</sup> NaOH ethanol solution was dropwise added to the mixed solution. The solution was then heated at 60 °C until complete ethanol volatilization, leaving behind a precipitate. This collected precipitate was rapidly heated to 723 K (10 K/min) and calcinated at 723 K for 120 minutes in a furnace under air conditions, resulting in the formation of black powder catalysts. The resulting  $\text{Tm}_{0.1}\text{Sb}_{0.2}\text{Ir}_{0.7}\text{O}_x@\text{TB-IrO}_x$  catalyst was thus obtained. For the synthesis of  $\text{Tm}_{0.1}\text{Ir}_{0.9}\text{O}_x@\text{TB-IrO}_x$ , and  $\text{Sb}_{0.2}\text{Ir}_{0.8}\text{O}_x@\text{TB-IrO}_x$ , the same method was followed, with the only difference being the alteration of the thulium chloride hexahydrate amount to 3.16 mg, and antimony trichloride amount to 3.76 mg respectively. The rapid heating and pyrolysis processes were found to play a crucial role in the fabrication of these nanocatalysts.

### **Characterizations**

For transmission electron microscopy (TEM), high-resolution TEM (HR-TEM) imaging, and energy-dispersive X-ray (EDX) spectroscopy, micrographs were obtained using a Tecnai

G2 F20 S-TWIN (FEI, America) equipped with an X-ray energy dispersive spectrometer with a field emission source at 200 keV. X-ray diffraction (XRD) analysis was performed on the crystal structures of the samples using a Bruker D8 Venture X-ray diffractometer with Cu-K $\alpha$  ( $\lambda = 1.54178 \text{ \AA}$ ) as the radiation source. X-ray photoelectron spectroscopy (XPS) was conducted on the surface nanocatalysts using VG ESCALAB with a monochrome Al anode (Al K $\alpha = 1486.6 \text{ eV}$ ). The multi-element content of the as-synthesized sample was determined by inductively coupled plasma (ICP) using an Agilent 7700 ICP-MS.

### ***Electrochemical Measurements***

Electrochemical characterizations, including cyclic voltammetry (CV), linear sweep voltammetry (LSV), and chronopotentiometry, were performed using a Bio-Logic VSP potentiostat with a three-electrode electrochemical system. For the oxygen evolution reaction (OER) test, a 0.5 M H<sub>2</sub>SO<sub>4</sub> solution served as the electrolyte, with Hg/Hg<sub>2</sub>SO<sub>4</sub> and platinum column electrodes utilized as the reference and counter electrodes, respectively. To prepare the catalyst sample, it was dispersed in a solution consisting of 500  $\mu\text{L}$  of isopropanol and 100  $\mu\text{L}$  of Nafion (5%). The mixed solution was sonicated for 1 hour to achieve a homogeneous mixed slurry. The resulting mixed slurry was then dropped onto glass carbon electrode and allowed to air dry at room temperature, creating the working electrode. Prior to the test, 0.5 M H<sub>2</sub>SO<sub>4</sub> was purged with high-purity nitrogen for at least 30 minutes to ensure the removal of dissolved oxygen from the electrolyte.

The data obtained in acidic solution ( $E_{\text{Hg}/\text{Hg}_2\text{SO}_4}$ ) are all converted into relative  $E_{\text{RHE}}$  potential:

$$E_{\text{RHE}} = E_{\text{Hg}/\text{Hg}_2\text{SO}_4} + E^0_{(\text{Hg}/\text{Hg}_2\text{SO}_4)} + 0.0592 \times \text{pH} \quad (1)$$

The electrochemical impedance was acquired through electrochemical impedance

spectroscopy (EIS) over a frequency range of 0.01 Hz to 100,000 Hz, with an AC potential amplitude of 5 mV applied during the measurements. The value of  $R_s$ , representing the solution resistance, was determined by fitting the EIS data to an equivalent circuit using ZSimpWin software. To compensate for the impact of uncompensated solution resistance ( $R_s$ ), the potentials were iR-corrected using the following equation:

$$E_{iR\text{-corrected}} = E_{\text{applied}} - iR_s \quad (2)$$

Where  $i$  is current on the electrode.

The double-layer capacitance ( $C_{dl}$ ) is calculated from CV measurements by the equation:

$$C_{dl} = (J_a - J_c) / (2 \times \nu) = (|J_a| + |J_c|) / (2 \times \nu) = \Delta J / (2 \times \nu) \quad (3)$$

Where  $J_a$  and  $J_c$  are the anodic and cathodic current density recorded at the middle of the selected potential range and  $\nu$  is the sweep rate.

The ECSA of the catalysts were estimated from  $C_{dl}$  by the equation:

$$\text{ECSA} = A_0 \times C_{dl} / C_s \quad (4)$$

Where the  $C_s$ , assumed to 35  $\mu\text{F cm}^{-2}$  based on typical reported value, is the specific capacitance of the sample or the capacitance of an atomically smooth planar surface of the material per unit area under identical electrolyte conditions.  $A_0$  is the geometric surface area of the working electrode.

Specific activity (SA) and mass activity (MA) are used to calculate the OER catalytic activity of the catalysts based on the kinetic current at 0.9 V vs. RHE.

$$\text{SA} = J_K / (\text{ECSA} \times m_{Ir}) \quad (5)$$

$$\text{MA} = J_K / (m_{Ir}) \quad (6)$$

Where  $J_K$  and  $m_{Ir}$  are the kinetic current density and  $m_{Ir}$  is the Ir loading amount, respectively.

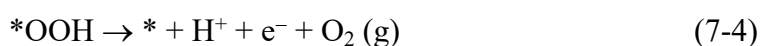
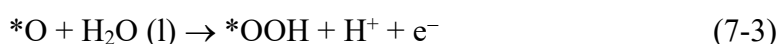
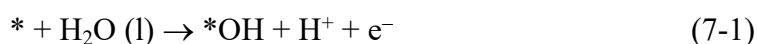
### ***Density function theory (DFT) calculation***

We have employed the Vienna Ab Initio Package (VASP)<sup>1, 2</sup> to perform all the spin-

polarized density functional theory (DFT) calculations within the generalized gradient approximation (GGA) using the Perdew-Burke-Ernzerhof (PBE)<sup>3</sup> formulation. We have chosen the projected augmented wave (PAW) potentials<sup>4</sup> to describe the ionic cores and take valence electrons into account using a plane wave basis set with a kinetic energy cutoff of 500eV. Partial occupancies of the Kohn–Sham orbitals were allowed using the Gaussian smearing method and a width of 0.10 eV. The electronic energy was considered self-consistent when the energy change was smaller than 10<sup>-5</sup> eV. The maximum Hellmann-Feynman force for each ionic optimization step is 0.01eV/Å, as well as the optimization of equilibrium lattice constants.

The configurations of catalysts are established, named IrO<sub>x</sub>, Sb-doped IrO<sub>2</sub> (three), Tm-doped IrO<sub>2</sub> (three), and Sb, Tm-doped IrO<sub>2</sub> (three), 1%, 2%, 4%, 6%, 8%. The p (4x4) unit cell was chose for those catalysts. This slab was separated by a 20 Å vacuum layer in the z direction between the slab and its periodic images. A 3×3×1 Monkhorst-Pack k-point grid for Brillouin zone sampling was used in structural optimization and energy calculation, and 5×5×1 Monkhorst-Pack k-point grid for density of state (DOS) simulation. Spin-polarization was considered in all calculations<sup>5</sup>. In order to fully consider the activity of each catalyst, the possible two catalytic sites in catalysts are selected to discuss their adsorption behavior.

The reaction mechanism of OER on various of catalysts have been identified to several elementary reaction steps:



The free energy ( $\Delta G$ ) of OER on those catalysts was defined as<sup>6</sup>

$$\Delta G = E_{\text{DFT}} + E_{\text{ZPE}} - T \times S \quad (8)$$

where  $E_{\text{DFT}}$ ,  $E_{\text{ZPE}}$ ,  $T$  and  $S$  are the calculation total energy of  $^*\text{O}$ ,  $^*\text{OH}$ , and  $^*\text{OOH}$  intermediate on catalysts surface, the zero-point energy, temperature, and entropy.

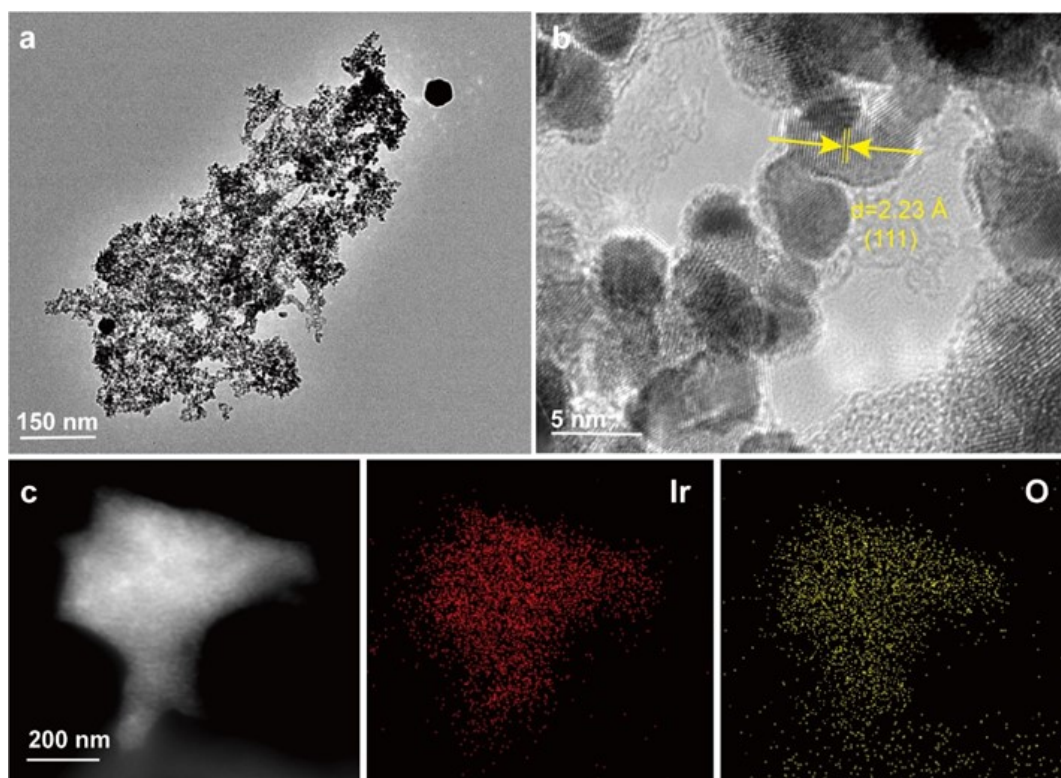
The overpotential ( $\eta^{\text{OER}}$ ) of OER was defined as<sup>7</sup>:

$$\eta^{\text{OER}} = \max(\Delta G_1, \Delta G_2, \Delta G_3, \Delta G_4)/e - 1.23 \quad (9)$$

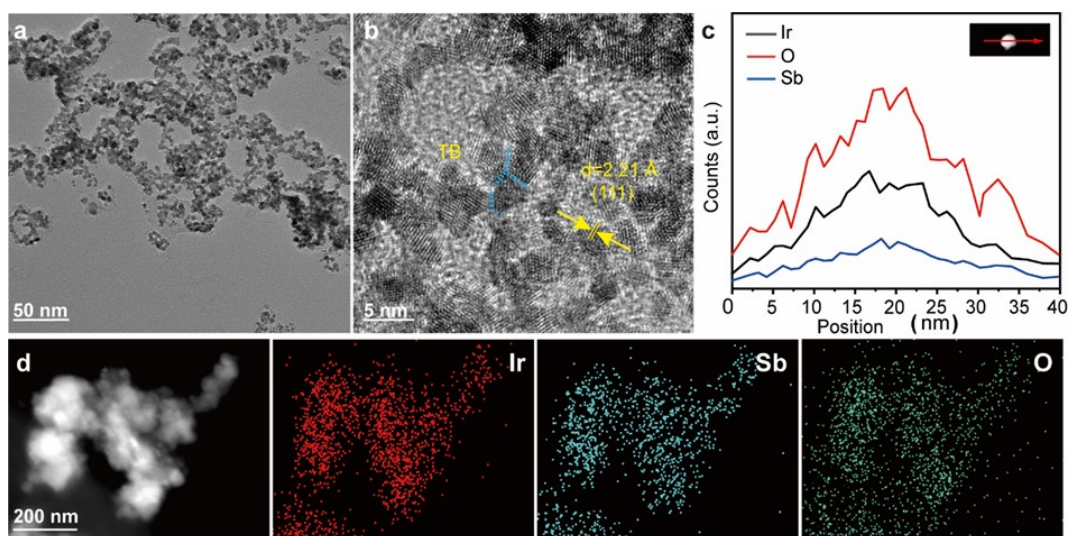
Where the  $\Delta G_1$ ,  $\Delta G_2$ ,  $\Delta G_3$ ,  $\Delta G_4$  are the free energy for four elementary reactions of OER.

### ***PEM electrolytic water***

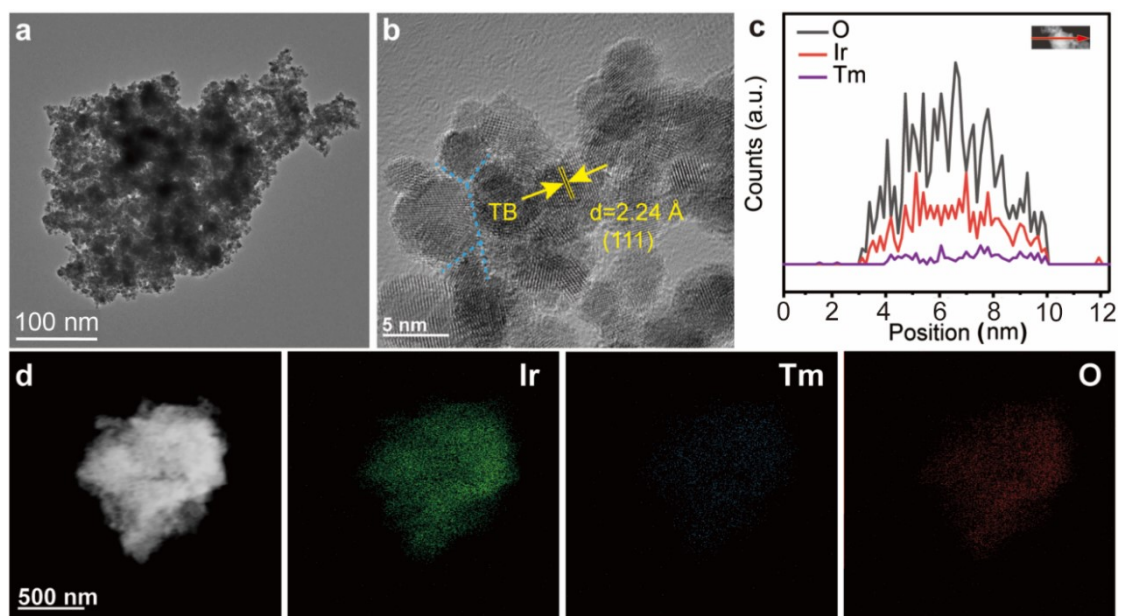
Nafion 117 membrane was heated at 80 °C in 0.5 M  $\text{H}_2\text{SO}_4$  for 30 minutes. Subsequently, the Nafion membrane was heated in a solution containing 3w%  $\text{H}_2\text{O}_2$  for an additional 30 minutes to remove the impurities. Finally, the membrane was immersed in ultra-pure water and heated for 30 minutes at 80 °C. The cathode catalyst Pt/C (20 wt%) was processed into an equal volume slurry following the same steps. The cathode catalyst was sprayed on the opposite side in an equivalent area. Finally, a carbon paper was placed on the cathode side of the Nafion 117 membrane, and titanium felt plated with Pt was placed on the anode side. The membrane electrode assembly was constructed by hot pressing at 150 °C and 10 MPa for 3 minutes. A well-dispersed slurry was prepared by combining 0.80 mg of nano-catalyst with a 1 mL solution of ethanol and water. After 4 hours of ultrasonic treatment, 100  $\mu\text{L}$  of 5 wt% Nafion solution was added. The Nafion 117 membrane was washed four times with ultra-pure water. The prepared anode catalyst, with a loading controlled at 0.31  $\text{mg cm}^{-2}$ , was sprayed on one side of the treated Nafion 117 membrane with an area of  $1 \times 1 \text{ cm}^2$ . The cathode catalyst Pt/C (20 wt%) was processed into an equal volume slurry following the same steps. The cathode catalyst was sprayed on the opposite side in an equivalent area.



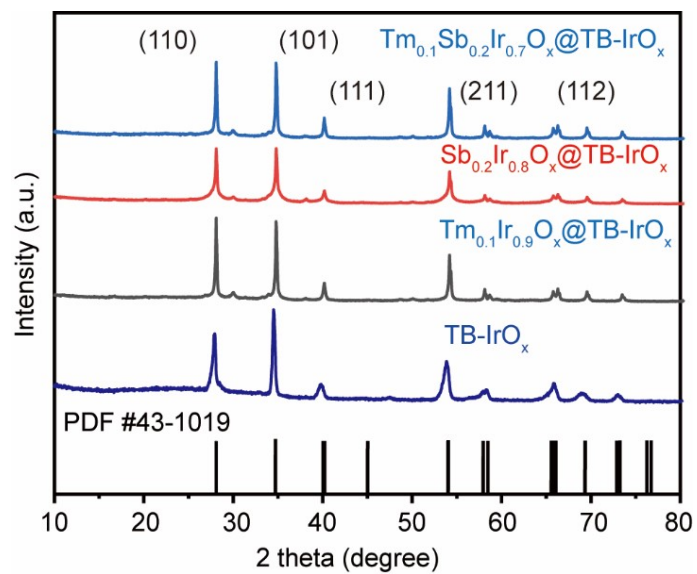
**Supplementary Figure 1.** (a) TEM image, (b) the HR-TEM image of IrO<sub>x</sub> and (c) the corresponding elemental mapping of IrO<sub>x</sub>.



**Supplementary Figure 2.** (a) TEM image, (b) the HR-TEM image of  $\text{Sb}_{0.2}\text{Ir}_{0.8}\text{O}_x@\text{TB-IrO}_x$ , (c) TEM-EDS line scan analysis and (d) the corresponding elemental mapping of  $\text{Sb}_{0.2}\text{Ir}_{0.8}\text{O}_x@\text{TB-IrO}_x$ .



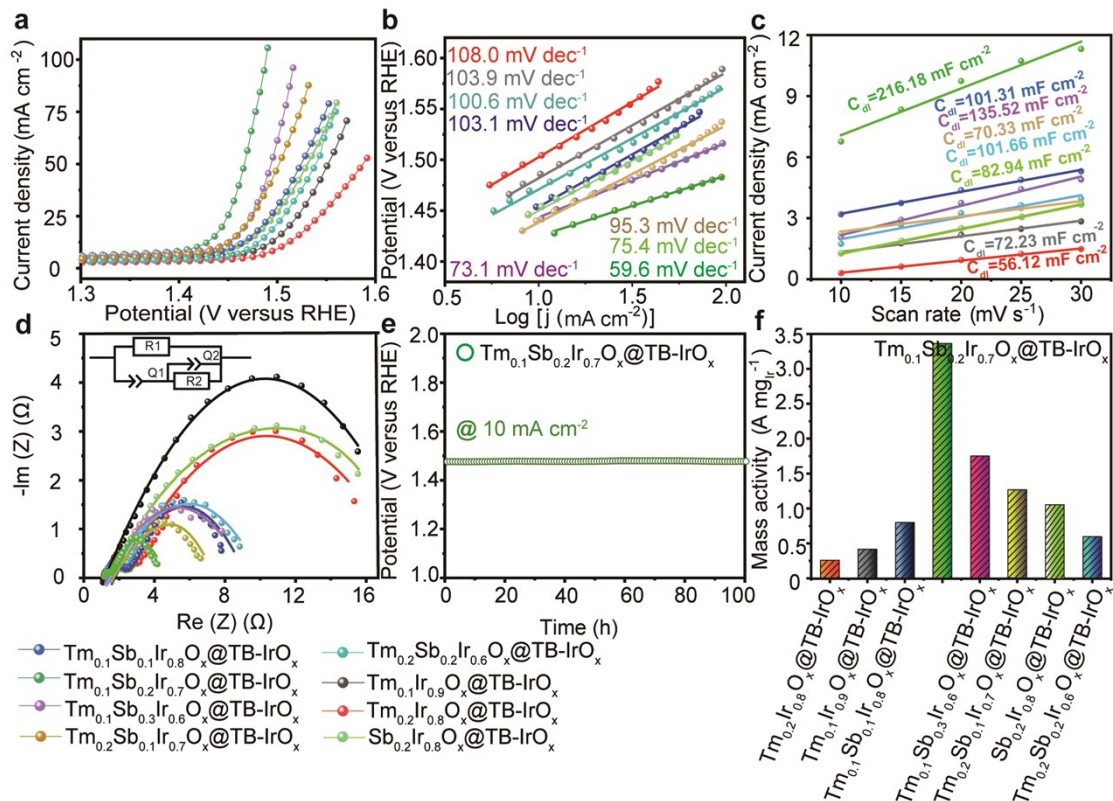
**Supplementary Figure 3.** (a) TEM image, (b) the HR-TEM image of  $\text{Tm}_{0.1}\text{Ir}_{0.9}\text{O}_x@TB\text{-IrO}_x$ , (c) TEM-EDS line scan analysis and (d) the corresponding elemental mapping of  $\text{Tm}_{0.1}\text{Ir}_{0.9}\text{O}_x@TB\text{-IrO}_x$ .



**Supplementary Figure 4.** XRD patterns of  $TB-IrO_x$ ,  $Tm_{0.1}Ir_{0.9}O_x@TB-IrO_x$ ,  $Sb_{0.2}Ir_{0.8}O_x@TB-IrO_x$  and  $Tm_{0.1}Sb_{0.2}Ir_{0.7}O_x@TB-IrO_x$  nanocatalysts.

**Supplementary Table 1.** The percentages of various valence state Ir in the various nanocatalysts.

Sample	Element	Area	%Area
C-IrO <sub>2</sub>	Ir <sup>4+</sup> 4f	29274.4	54.47%
	Ir <sup>4+</sup> 4f sat	24468.2	45.53%
TB-IrO <sub>x</sub>	Ir <sup>&lt;3+</sup> 4f	25560.5	24.80%
	Ir <sup>3+</sup> 4f	42989.5	41.71%
	Ir <sup>&gt;3+</sup> 4f	34529.6	33.49%
Tm <sub>0.1</sub> Ir <sub>0.9</sub> O <sub>x</sub> @TB-IrO <sub>x</sub>	Ir <sup>&lt;3+</sup> 4f	27143.6	34.14%
	Ir <sup>3+</sup> 4f	33321.5	41.91%
	Ir <sup>&gt;3+</sup> 4f	19037.6	23.95%
Sb <sub>0.2</sub> Ir <sub>0.8</sub> O <sub>x</sub> @TB-IrO <sub>x</sub>	Ir <sup>&lt;3+</sup> 4f	60652.6	36.25%
	Ir <sup>3+</sup> 4f	46545.1	27.82%
	Ir <sup>&gt;3+</sup> 4f	60108.1	35.93%
Tm <sub>0.1</sub> Sb <sub>0.2</sub> Ir <sub>0.7</sub> O <sub>x</sub> @TB-IrO <sub>x</sub>	Ir <sup>&lt;3+</sup> 4f	23178.2	20.48%
	Ir <sup>3+</sup> 4f	50357.3	41.12%
	Ir <sup>&gt;3+</sup> 4f	39660.2	38.40%
Tm <sub>0.1</sub> Sb <sub>0.2</sub> Ir <sub>0.7</sub> O <sub>x</sub> @TB-IrO <sub>x</sub> -post reaction	Ir <sup>&lt;3+</sup> 4f	37145.4	30.52%
	Ir <sup>3+</sup> 4f	42312.6	34.75%
	Ir <sup>&gt;3+</sup> 4f	42275.3	34.73%



**Supplementary Figure 5.** (a) LSV curves (b) Tafel plots (c) C<sub>dl</sub> and (d) EIS of various synthesized Tm<sub>n</sub>Sb<sub>m</sub>Ir<sub>1-m-n</sub>O<sub>x</sub>@TB-IrO<sub>x</sub> nanocatalysts collected in 0.5 M H<sub>2</sub>SO<sub>4</sub> electrolyte. (e) Chronopotentiometry curve of Tm<sub>0.1</sub>Sb<sub>0.2</sub>Ir<sub>0.7</sub>O<sub>x</sub>@TB-IrO<sub>x</sub> nanocatalysts operated at 10 mA cm<sup>-2</sup>. (f) Mass activities of these nanocatalysts at η = 270 mV.

**Supplementary Table 2.** Comparisons of  $\text{Tm}_{0.1}\text{Sb}_{0.2}\text{Ir}_{0.7}\text{O}_x@\text{TB-IrO}_x$  with other representative OER catalysts reported under acidic condition.

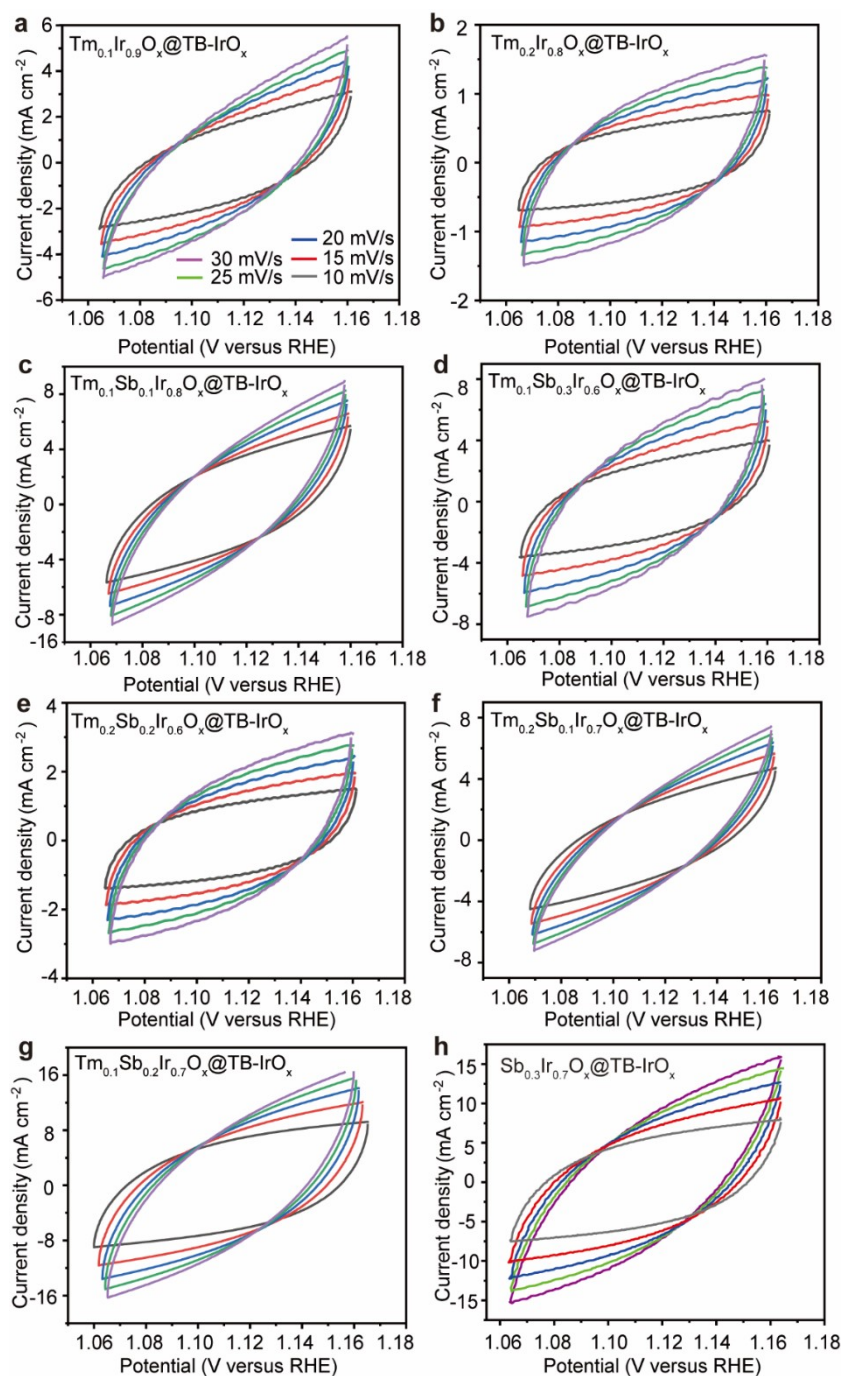
Catalysts	Stability (h)	Overpotentials at the corresponding $j$ (10 $\text{mA cm}^{-2}$ )	Reference
Co-RuIr	25	$\eta_{10} = 235 \text{ mV}$	<i>Adv. Mater.</i> , 31, e1900510 (2019)
$\text{Rh}_{22}\text{Ir}_{78}$ alloy	2000 <sup>th</sup> cycle	$\eta_{10} = 292 \text{ mV}$	<i>ACS Nano</i> , 13, 13225-13234 (2019)
Ir- $\text{Co}_3\text{O}_4$	6	$\eta_{10} = 236 \text{ mV}$	<i>Nat. Commun.</i> , 13, 7754 (2022)
$\text{IrO}_x/\text{Zr}_2\text{ON}_2$	5	$\eta_{10} = 255 \text{ mV}$	<i>Adv. Funct. Mater.</i> , 2301557 (2023)
IrRu@Te	20	$\eta_{10} = 220 \text{ mV}$	<i>ACS Catal.</i> , 10, 3571-3579 (2020)
3C-SrIrO <sub>3</sub> (or IrO <sub>x</sub> /SrIrO <sub>3</sub> )	20	$\eta_{10} = 270\text{-}290 \text{ mV}$	<i>Science</i> , 353, 1011 (2016)
IrCo@IrO <sub>x</sub> -3L	8	$\eta_{10} = 247 \text{ mV}$	<i>Adv. Mater.</i> , 31, (2019)
$\text{Pt}_{0.1}\text{La}_{0.1}\text{-IrO}_2@\text{NC}$	135	$\eta_{10} = 205 \text{ mV}$	<i>Appl. Catal. B: Environ.</i> , 266, 118643 (2020)
$\text{H}_x\text{IrO}_3$	12	$\eta_{10} = 277 \text{ mV}$	<i>ACS Appl. Energy Mater.</i> , 5, 6869-6877 (2022)
RuIrO <sub>x</sub>	24	$\eta_{10} = 233 \text{ mV}$	<i>Nat. Commun.</i> , 10, 4875 (2019)
$\text{Ce}_{0.2}\text{-IrO}_2@\text{NPC}$	100	$\eta_{10} = 224 \text{ mV}$	<i>ACS Appl. Mater. Interfaces</i> , 12, 37006-37012 (2020)
IrMoO <sub>x</sub>	30	$\eta_{10} = 267 \text{ mV}$	<i>Chem. Eng. J.</i> , 440, 135851 (2022)

IrO <sub>2</sub> @Co <sub>3</sub> O <sub>4</sub> - CoMoO <sub>4</sub>	36	$\eta_{10} = 236$ mV	<i>Chem. Eng. J.</i> , 473, 145353 (2023)
Ru@Ir-O	40	$\eta_{10} = 238$ mV	<i>Small</i> , 18, 2108031 (2022)
IrO <sub>x</sub> /CeO <sub>2</sub>	300	$\eta_{10} = 220$ mV	<i>Nano Energy</i> , 104, 107960 (2022)
Ir <sub>0.7</sub> W <sub>0.2</sub> Sn <sub>0.1</sub> O <sub>x</sub>	220	$\eta_{10} = 236$ mV	<i>Small</i> , 18, 2203365 (2022)
CeO <sub>2</sub> @SrIrO <sub>3</sub>	50	$\eta_{10} = 238$ mV	<i>Appl. Catal. B: Environ.</i> , 315, 121579 (2022)
This work	100	$\eta_{10} = 192$ mV	-

---

**Supplementary Table 3.** Comparisons of  $\text{Tm}_{0.1}\text{Sb}_{0.2}\text{Ir}_{0.7}\text{O}_x@TB\text{-IrO}_x$  with other representative OER catalysts reported under acidic condition at  $100 \text{ mA cm}^{-2}$ .

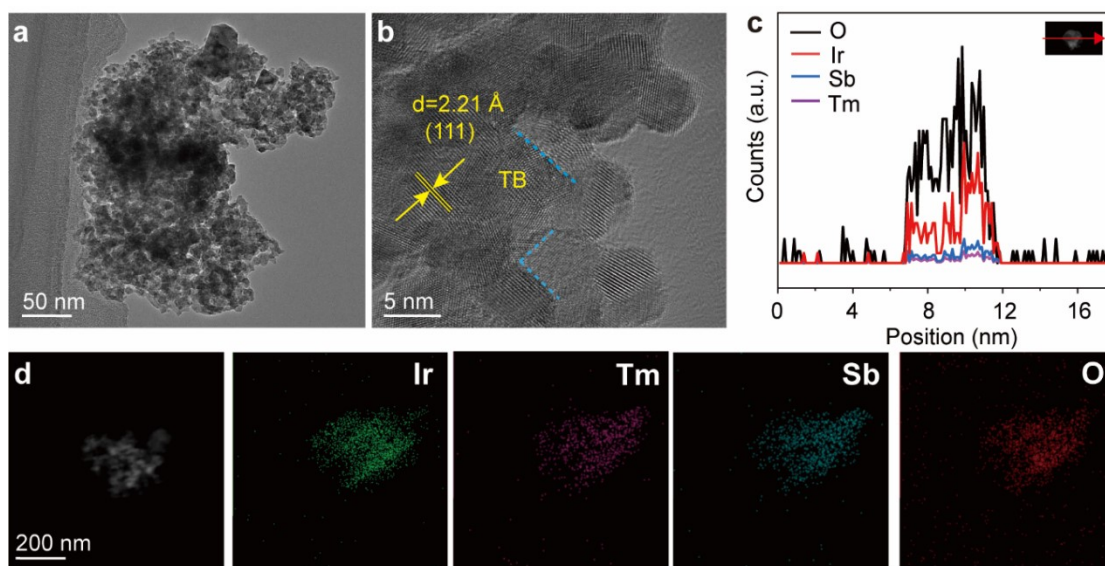
Catalysts	Overpotentials at the corresponding $j$ ( $100 \text{ mA cm}^{-2}$ )	Reference
sl- $\text{Mn}_{0.98}\text{Ir}_{0.02}\text{O}_2$	$\eta_{100} = 277 \text{ mV}$	<i>Adv. Mater.</i> , 35, 2308060 (2023)
3R- $\text{IrO}_2$	$\eta_{100} = 260 \text{ mV}$	<i>Joule</i> , 5, 3221-3234 (2021)
$\text{Ru}@Ir\text{-O}$	$\eta_{100} = 350 \text{ mV}$	<i>Small</i> , 18, 2108031 (2022) <i>ACS Appl. Mater. Interfaces</i> , 12, 37006-37012 (2020)
$\text{Ce}_{0.2}\text{-IrO}_2@NPC$	$\eta_{100} = 280 \text{ mV}$	<i>Nat. Nanotechnol.</i> , 16, 1371-1377 (2021)
GB- $\text{Ta}_{0.1}\text{Tm}_{0.1}\text{Ir}_{0.8}\text{O}_{2-\delta}$	$\eta_{100} = 265 \text{ mV}$	<i>ACS Catal.</i> , 11, 3402-3413 (2021)
$\text{RuIr}@CoNC$	$\eta_{100} = 300 \text{ mV}$	<i>Small</i> , 18, 2203365 (2022)
$\text{Ir}_{0.7}\text{W}_{0.2}\text{Sn}_{0.1}\text{O}_x$	$\eta_{100} = 292 \text{ mV}$	<i>Nano Research</i> , 15, 5933-5939 (2022)
$\text{Ir}_x\text{Ru}_{1-x}\text{O}_2$	$\eta_{100} = 250 \text{ mV}$	<i>Adv. Funct. Mater.</i> , 33, 2301557 (2023)
$\text{IrO}_x/\text{Zr}_2\text{ON}_2$	$\eta_{100} = 300 \text{ mV}$	<i>ACS Catal.</i> , 13, 4120-4126 (2023)
2D fcc- $\text{Ru}_3\text{Ir}$	$\eta_{100} = 260 \text{ mV}$	-
This work	$\eta_{100} = 250 \text{ mV}$	-



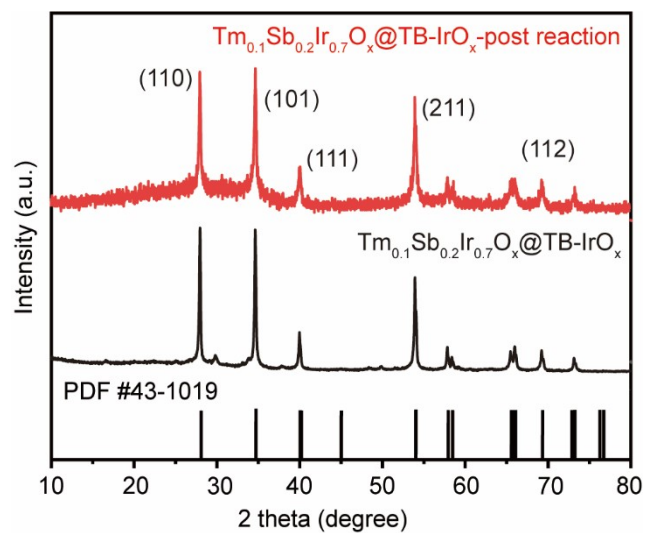
**Supplementary Figure 6.** CV curves of various nanocatalysts collected at different scan rates in 0.5 M H<sub>2</sub>SO<sub>4</sub> electrolyte.

**Supplementary Table 4.** ICP analysis of leached metal elements from the  $\text{Tm}_{0.1}\text{Sb}_{0.2}\text{Ir}_{0.7}\text{O}_x@/\text{TB-IrO}_x$  after OER stability test in 0.5 M  $\text{H}_2\text{SO}_4$  at 10  $\text{mA cm}^{-2}$ .

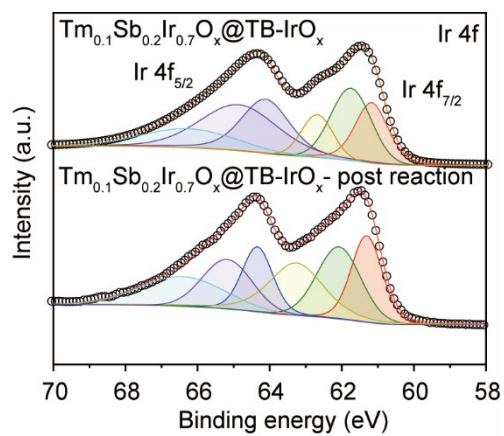
Element	Ion concentrations in electrolyte after 100 h (ppb)	Mass loss ratio of catalyst (wt%)
Ir	10.56	0.19
Sb	37.32	0.68
Tm	25.91	0.47



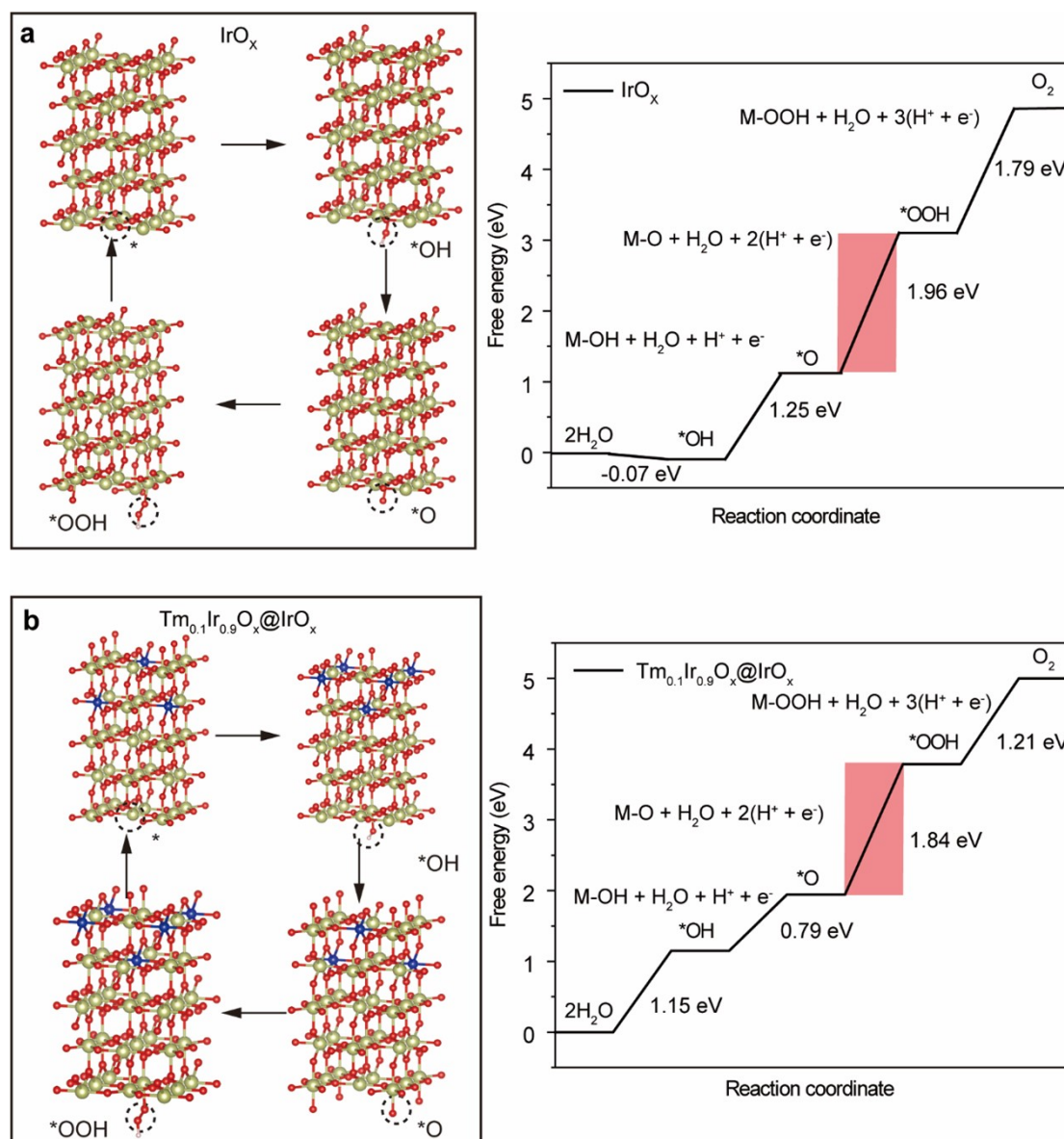
**Supplementary Figure 7.** (a) TEM image, (b) the HR-TEM image of  $\text{Tm}_{0.1}\text{Sb}_{0.2}\text{Ir}_{0.7}\text{O}_x@TB\text{-IrO}_x$ -post reaction, (c) EDS elemental concentration profiles along the red scan line, and (d) the corresponding elemental mapping of  $\text{Tm}_{0.1}\text{Sb}_{0.2}\text{Ir}_{0.7}\text{O}_x@TB\text{-IrO}_x$ -post reaction.



**Supplementary Figure 8.** XRD patterns of  $\text{Tm}_{0.1}\text{Sb}_{0.2}\text{Ir}_{0.7}\text{O}_x$ @TB-IrO<sub>x</sub> and  $\text{Tm}_{0.1}\text{Sb}_{0.2}\text{Ir}_{0.7}\text{O}_x$ @TB-IrO<sub>x</sub>-post reaction nanocatalysts.

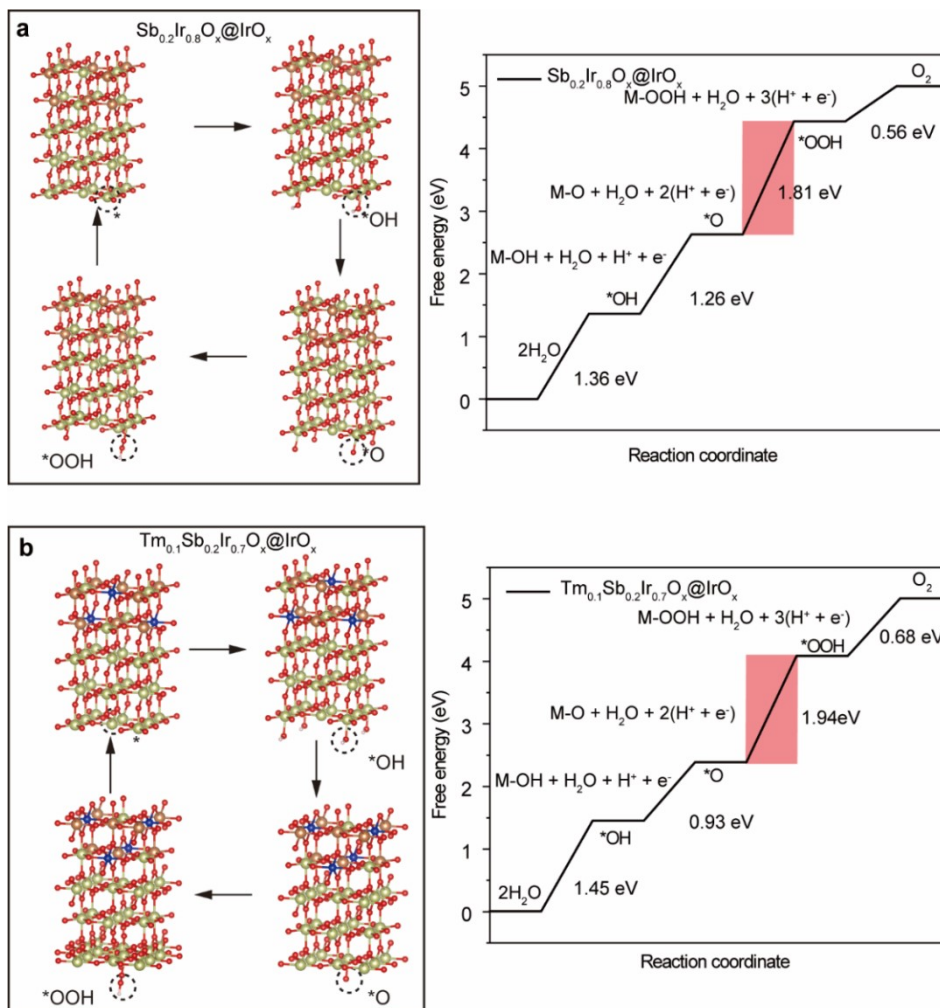


**Supplementary Figure 9.** Ir 4f XPS spectra for  $\text{Tm}_{0.1}\text{Sb}_{0.2}\text{Ir}_{0.7}\text{O}_x@TB\text{-IrO}_x$  and  $\text{Tm}_{0.1}\text{Sb}_{0.2}\text{Ir}_{0.7}\text{O}_x@TB\text{-IrO}_x$ -post reaction nanocatalysts.

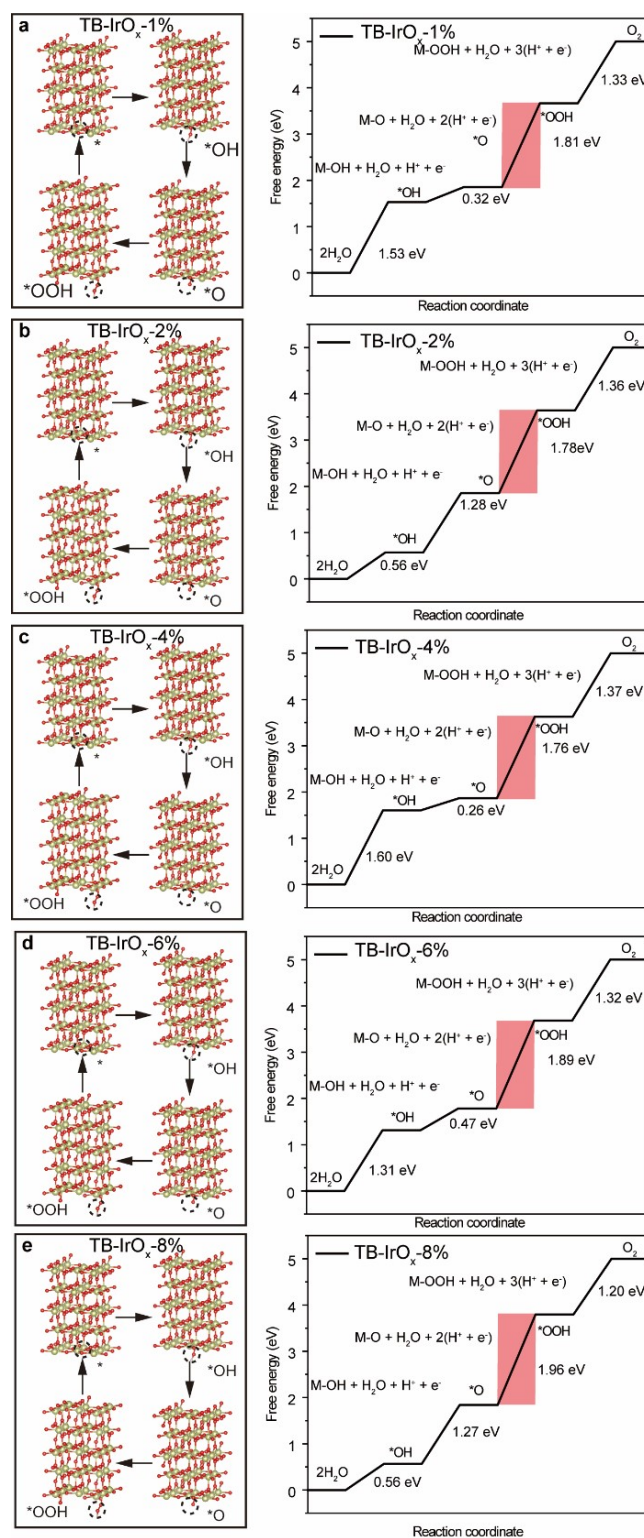


**Supplementary Figure 10.** The calculated DFT energetics of  $\text{IrO}_x$  and  $\text{Tm}_{0.1}\text{Ir}_{0.9}\text{O}_x@ \text{IrO}_x$  surfaces toward acidic OER reaction steps (a-b). The established models toward acidic OER on the  $\text{IrO}_x$  and  $\text{Tm}_{0.1}\text{Ir}_{0.9}\text{O}_x@ \text{IrO}_x$ , respectively (yellow: Ir; red: O; pink: H; blue: Tm) and the free energies calculated at  $U = 0$  toward acidic OER reaction steps on the  $\text{IrO}_x$  and  $\text{Tm}_{0.1}\text{Ir}_{0.9}\text{O}_x@ \text{IrO}_x$ , respectively. The red box is the potential determination step (PDS).

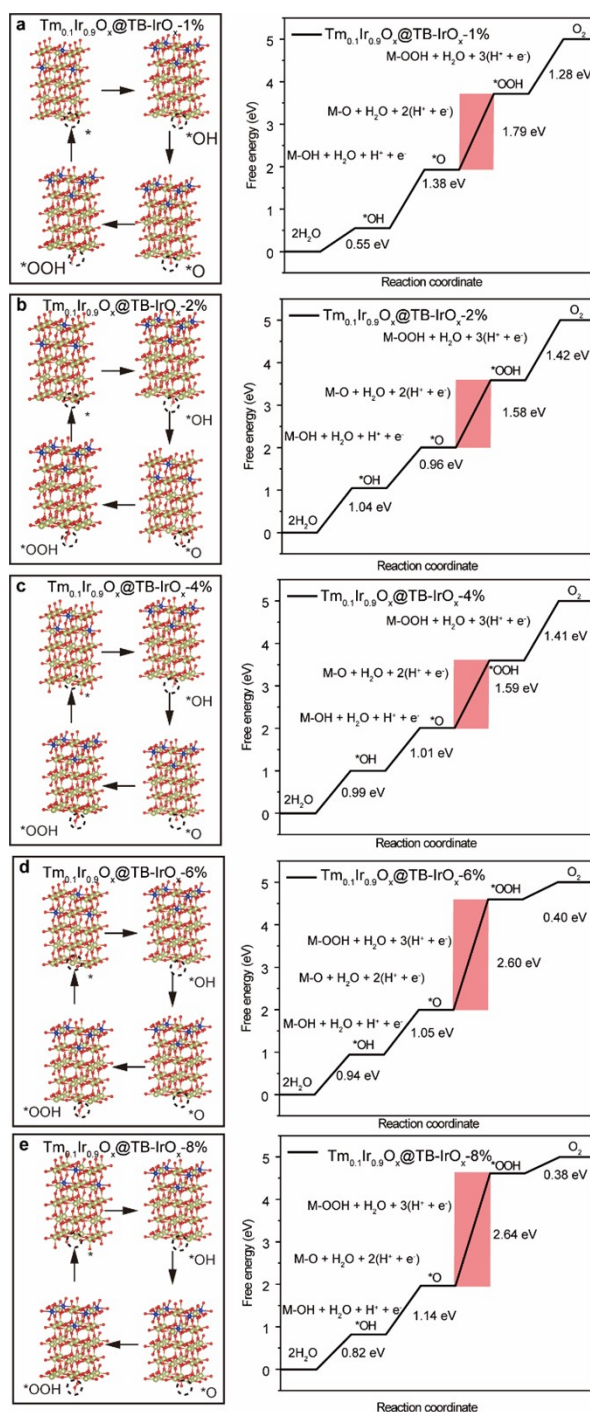
The DFT calculations for  $\text{IrO}_x$  and  $\text{Tm}_{0.1}\text{Ir}_{0.9}\text{O}_x@ \text{IrO}_x$  surfaces were all established and calculated at  $U=0$  V. On these  $\text{IrO}_x$  surfaces, the free energy barrier ( $\Delta G$ ) associated with the transformation of  $\text{O}^*$  to  $\text{OOH}^*$  was the potential determining step (PDS) of OER.



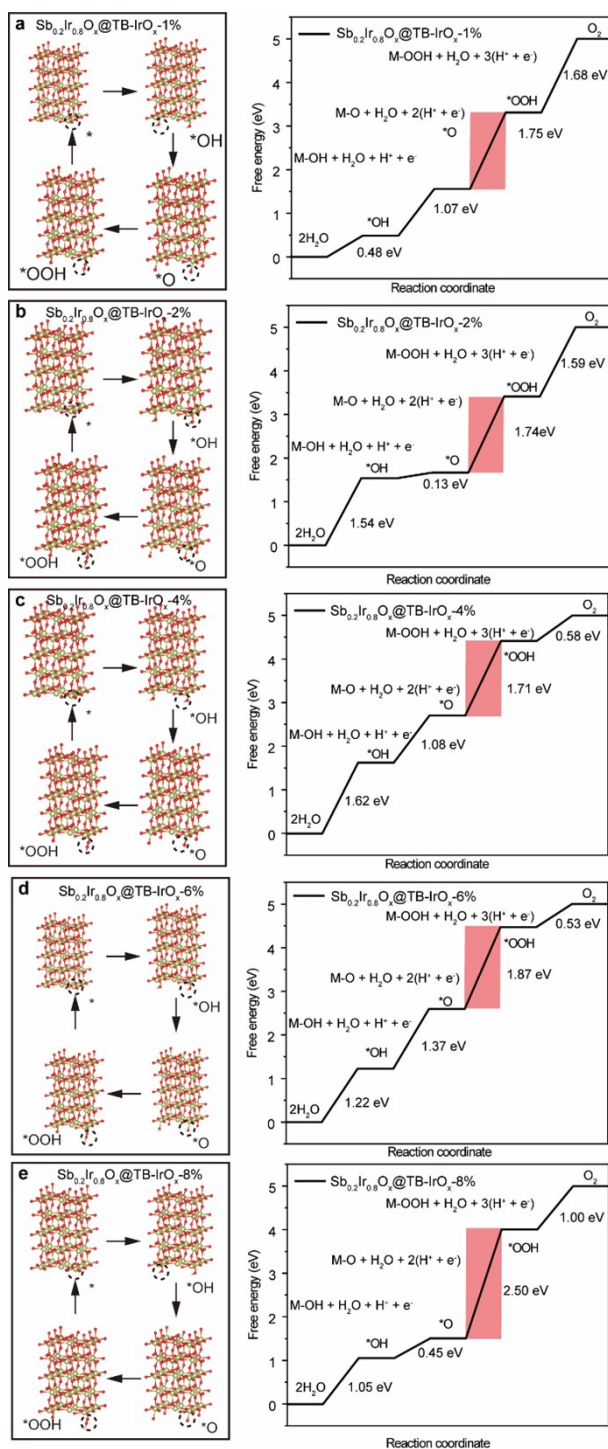
**Supplementary Figure 11.** The calculated DFT energetics of  $\text{Sb}_{0.2}\text{Ir}_{0.8}\text{O}_x@\text{IrO}_x$  and  $\text{Tm}_{0.1}\text{Sb}_{0.2}\text{Ir}_{0.7}\text{O}_x@\text{IrO}_x$  surfaces toward acidic OER reaction steps (a-b). The established models toward acidic OER on the  $\text{Sb}_{0.2}\text{Ir}_{0.8}\text{O}_x@\text{IrO}_x$  and  $\text{Tm}_{0.1}\text{Sb}_{0.2}\text{Ir}_{0.7}\text{O}_x@\text{IrO}_x$ , respectively (yellow: Ir; red: O; brown: Sb; blue: Tm) and the free energies calculated at  $U = 0$  toward acidic OER reaction steps on the  $\text{Sb}_{0.2}\text{Ir}_{0.8}\text{O}_x@\text{IrO}_x$  and  $\text{Tm}_{0.1}\text{Sb}_{0.2}\text{Ir}_{0.7}\text{O}_x@\text{IrO}_x$ , respectively. The red box is the potential determination step (PDS).



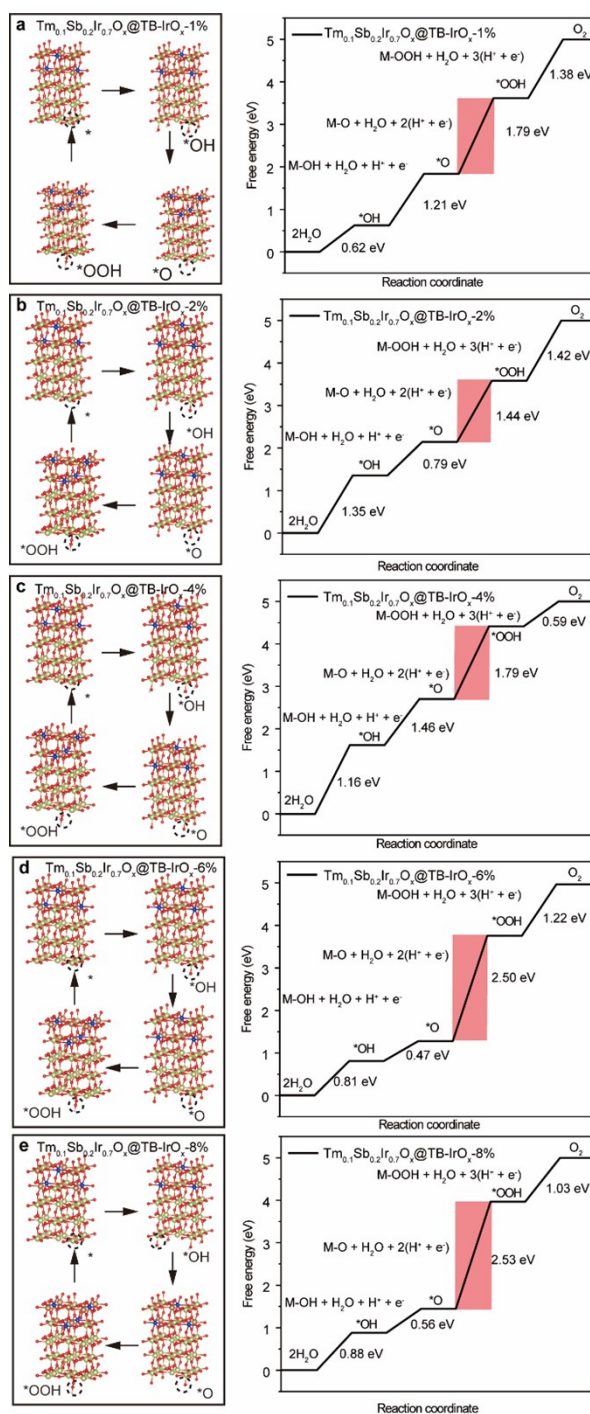
**Supplementary Figure 12.** The calculated DFT energetics of TB-IrO<sub>x</sub> (1%, 2%, 4%, 6%, 8%) surfaces toward acidic OER reaction steps (a-e). The established models toward acidic OER on the TB-IrO<sub>x</sub> (1%, 2%, 4%, 6%, 8%), respectively (yellow: Ir; red: O; pink: H; blue: Tm) and the free energies calculated at U = 0 toward acidic OER reaction steps on the TB-IrO<sub>x</sub> (1%, 2%, 4%, 6%, 8%), respectively. The red box is the potential determination step (PDS).



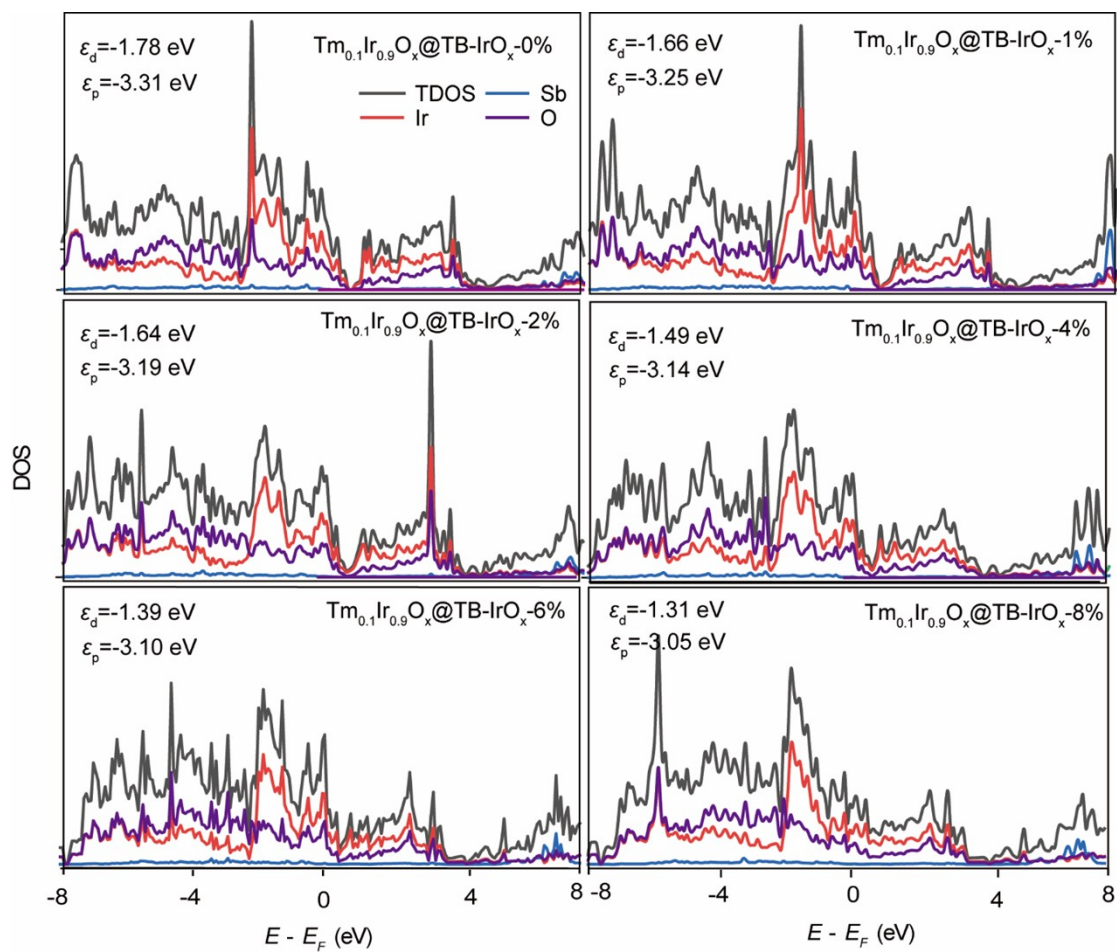
**Supplementary Figure 13.** The calculated DFT energetics of  $Tm_{0.1}Ir_{0.9}O_x@TB-IrO_x$  (1%, 2%, 4%, 6%, 8%) surfaces toward acidic OER reaction steps (a-e). The established models toward acidic OER on the  $Tm_{0.1}Ir_{0.9}O_x@TB-IrO_x$  (1%, 2%, 4%, 6%, 8%), respectively (yellow: Ir; red: O; pink: H; blue: Tm) and the free energies calculated at  $U = 0$  toward acidic OER reaction steps on the  $Tm_{0.1}Ir_{0.9}O_x@TB-IrO_x$  (1%, 2%, 4%, 6%, 8%), respectively. The red box is the potential determination step (PDS).



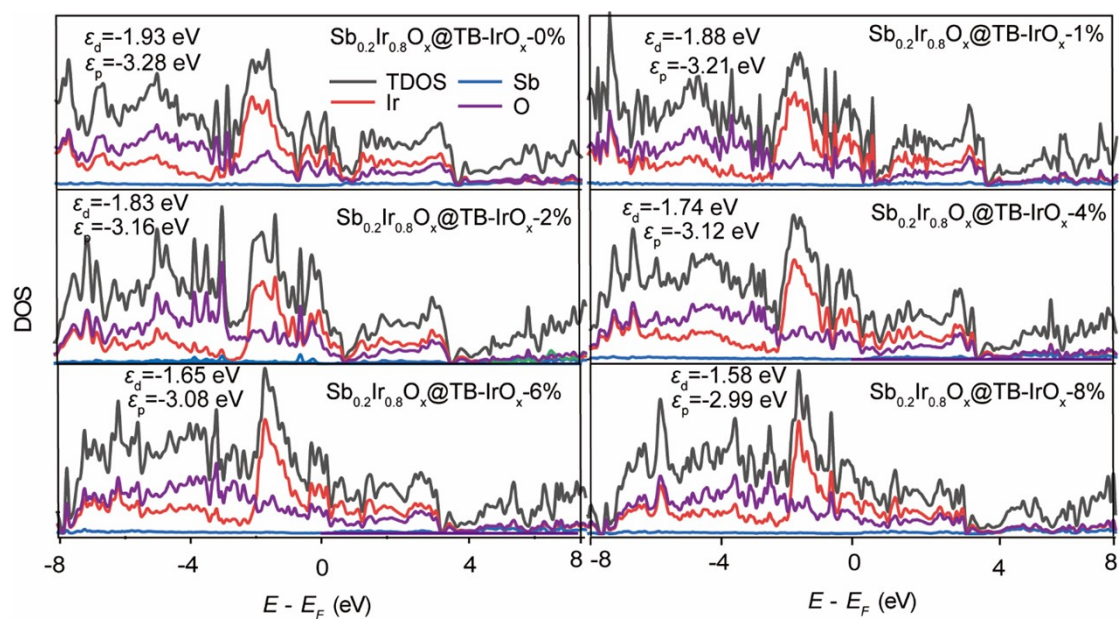
**Supplementary Figure 14.** The calculated DFT energetics of  $\text{Sb}_{0.2}\text{Ir}_{0.8}\text{O}_x@TB\text{-IrO}_x$  (1%, 2%, 4%, 6%, 8%) surfaces toward acidic OER reaction steps (a-e). The established models toward acidic OER on the  $\text{Sb}_{0.2}\text{Ir}_{0.8}\text{O}_x@TB\text{-IrO}_x$  (1%, 2%, 4%, 6%, 8%), respectively (yellow: Ir; red: O; pink: H; blue: Tm) and the free energies calculated at  $U = 0$  toward acidic OER reaction steps on the  $\text{Sb}_{0.2}\text{Ir}_{0.8}\text{O}_x@TB\text{-IrO}_x$  (1%, 2%, 4%, 6%, 8%), respectively. The red box is the potential determination step (PDS).



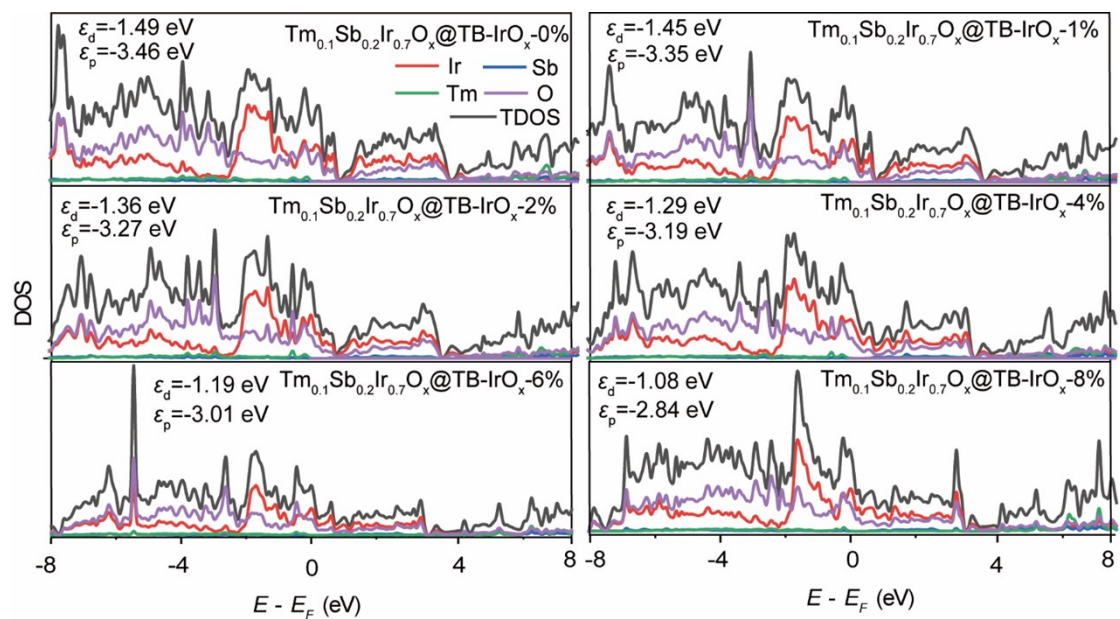
**Supplementary Figure 15.** The calculated DFT energetics of  $Tm_{0.1}Sb_{0.2}Ir_{0.7}O_x@TB-IrO_x$  (1%, 2%, 4%, 6%, 8%) surfaces toward acidic OER reaction steps (a-e). The established models toward acidic OER on the  $Tm_{0.1}Sb_{0.2}Ir_{0.7}O_x@TB-IrO_x$  (1%, 2%, 4%, 6%, 8%), respectively (yellow: Ir; red: O; pink: H; blue: Tm) and the free energies calculated at  $U = 0$  toward acidic OER reaction steps on the  $Tm_{0.1}Sb_{0.2}Ir_{0.7}O_x@TB-IrO_x$  (1%, 2%, 4%, 6%, 8%), respectively. The red box is the potential determination step (PDS).



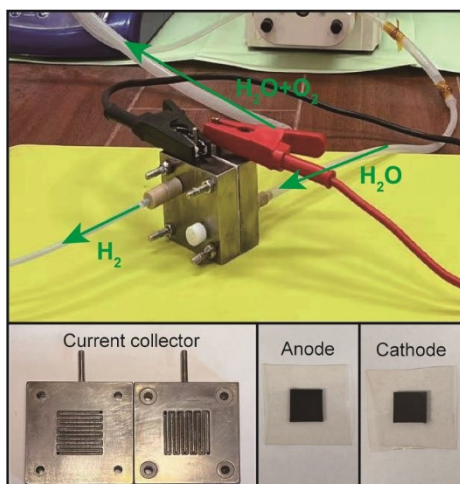
**Supplementary Figure 16.** Projected density of state (DOS) of  $\text{Tm}_{0.1}\text{Ir}_{0.9}\text{O}_x @ \text{TB-IrO}_x$  (0%, 1%, 2%, 4%, 6%, 8%).



**Supplementary Figure 17.** Projected density of state (DOS) of  $\text{Sb}_{0.2}\text{Ir}_{0.8}\text{O}_x@TB\text{-IrO}_x$  (0%, 1%, 2%, 4%, 6%, 8%).



**Supplementary Figure 18.** Projected density of state (DOS) of  $\text{Tm}_{0.1}\text{Sb}_{0.2}\text{Ir}_{0.7}\text{O}_x @ \text{TB-IrO}_x$  (0%, 1%, 2%, 4%, 6%, 8%).



**Supplementary Figure 19.** Image of PEM electrolyzer and membrane electrode after operation and disassembly.

**Supplementary Table 5.** Under the condition that all metal atoms are active for OER, the TOF values of various  $\text{Tm}_n\text{Sb}_m\text{Ir}_{1-m}\text{O}_x@ \text{TB-IrO}_x$  anode catalysts in the PEM electrolyzer.

Catalysts	Molecular weight (g mol <sup>-1</sup> )	Mol (unit cm <sup>-2</sup> )	TOF (O <sub>2</sub> s <sup>-1</sup> )
TB-IrO <sub>x</sub>	224.2	$1.62 \times 10^{18}$	1.44
Tm <sub>0.1</sub> Ir <sub>0.9</sub> O <sub>x</sub> @TB-IrO <sub>x</sub>	221.8	$1.45 \times 10^{18}$	1.61
Sb <sub>0.2</sub> Ir <sub>0.8</sub> O <sub>x</sub> @TB-IrO <sub>x</sub>	210.1	$1.37 \times 10^{18}$	1.71
Tm <sub>0.1</sub> Sb <sub>0.2</sub> Ir <sub>0.7</sub> O <sub>x</sub> @TB-IrO <sub>x</sub>	207.8	$1.22 \times 10^{18}$	1.92

**Supplementary Table 6.** Under the condition that only the metal atoms on the particle surface are active for OER, the TOF values of various  $\text{Tm}_n\text{Sb}_m\text{Ir}_{1-m}\text{O}_x@ \text{TB-IrO}_x$  anode catalysts in PEM.

Catalysts	Number of atoms in sphere	Correction of TOF by 15.7%
TB-IrO <sub>x</sub>	$1.5 \times 10^4$	9.17
$\text{Tm}_{0.1}\text{Ir}_{0.9}\text{O}_x@ \text{TB-IrO}_x$	$1.5 \times 10^4$	10.25
$\text{Sb}_{0.2}\text{Ir}_{0.8}\text{O}_x@ \text{TB-IrO}_x$	$1.5 \times 10^4$	10.89
$\text{Tm}_{0.1}\text{Sb}_{0.2}\text{Ir}_{0.7}\text{O}_x@ \text{TB-IrO}_x$	$1.5 \times 10^4$	12.23

**Supplementary Table 7.** The power and efficiency of the PEM electrolyzer employing various  $\text{Tm}_n\text{Sb}_m\text{Ir}_{1-m}\text{O}_x@TB\text{-IrO}_x$  anode catalysts operated at  $2.0 \text{ A cm}^{-2}$ .

Catalysts	Electrolyzer Power ( $\text{W cm}^{-2}$ )	Efficiency
TB-IrO <sub>x</sub>	4.73	52.01%
Tm <sub>0.1</sub> Ir <sub>0.9</sub> O <sub>x</sub> @TB-IrO <sub>x</sub>	4.42	55.7%
Sb <sub>0.2</sub> Ir <sub>0.8</sub> O <sub>x</sub> @TB-IrO <sub>x</sub>	4.28	57.5%
Tm <sub>0.1</sub> Sb <sub>0.2</sub> Ir <sub>0.7</sub> O <sub>x</sub> @TB-IrO <sub>x</sub>	4.02	61.5%

## References

- [1] Kresse, G.; Furthmüller, J. Efficiency of ab-initio total energy calculations for metals and semiconductors using a plane-wave basis set, *Comput. Mater. Sci.*, 1996, **6**, 15-50.
- [2] Kresse, G.; Furthmüller, J. Efficient iterative schemes for ab initio total-energy calculations using a plane-wave basis set, *Phys. Rev. B*, 1996, **54**, 11169-11186.
- [3] Perdew, J. P.; Burke, K.; Ernzerhof, M. Generalized Gradient Approximation Made Simple. *Phys. Rev. Lett.*, 1996, **77**, 3865-3868.
- [4] Kresse, G.; Joubert, D. From ultrasoft pseudopotentials to the projector augmented-wave method. *Phys. Rev. B*, 1999, **59**, 1758-1775.
- [5] Gong, L. Catalytic Mechanisms and Design Principles for Single-Atom Catalysts in Highly Efficient CO<sub>2</sub> Conversion, *Adv. Energy Mater.*, 2019 **9**, 1902625.
- [6] Zhao, Z.; Xia, Z. Design Principles for Dual-Element-Doped Carbon Nanomaterials as Efficient Bifunctional Catalysts for Oxygen Reduction and Evolution Reactions. *Acs Catal.*, 2016, **6**, 1553-1558.
- [7] Zhang, L. Guiding Principles for Designing Highly Efficient Metal-Free Carbon Catalysts. *Adv. Mater.*, 2019, **31**, 1805252.